Eur. Phys. J. AP **6**, 1–6 (1999)

THE EUROPEAN PHYSICAL JOURNAL APPLIED PHYSICS

Atomic force microscopy of twin formation in low-stacking fault CuAl alloy

C. Coupeau[a], F. Tranchant, J. Vergnol, and J. Grilhé

Laboratoire de Métallurgie-Physique, Université de Poitiers, B.P. 179, 86960 Futuroscope Cedex, France

Received: 31 March 1998 / Revised: 24 September 1998 / Accepted: 1st December 1998

Abstract. CuAl single crystals of a low stacking fault energy have been deformed along the ⟨111⟩ direction in an apparatus which consists of a compression machine interfaced with an atomic force microscope. The emergence process of dislocations has been in situ studied during deformation. Plasticity occurs in this material by propagation of Shockley dislocations which generate two possible kinds of stacking faults, extrinsic or intrinsic. The fine structure of slip lines has been investigated by atomic force microscopy. A differentiation between these two possible twin mechanisms in this alloy is attempted. It is concluded that twinning in this material can not only be explained by the intrinsic stacking faults and that the contribution of extrinsic faults has to be considered.

PACS. 61.16.Ch Scanning probe microscopy: scanning tunneling, atomic force, scanning optical, magnetic force, etc. – 68.35.Bs Surface structure and topography – 61.72.Nn Stacking faults and other planar or extended defects

1 Introduction

In pure copper (stacking fault energy $\gamma = 50$ mJ/m^2) and in copper-19 atomic% aluminium solid solution alloy ($\gamma = 5$ mJ/m^2), plastic deformation involves propagation in the bulk crystal of Shockley dislocations which generate two possible kinds of stacking faults, extrinsic or intrinsic. Moreover in these FCC alloys, twinning mechanisms occur only along the ⟨111⟩ direction in tension and ⟨100⟩ in compression and start both when the applied stress reaches a critical value corresponding to a large plastic strain [1,2]. The authors have shown that, in both cases, the stress applied on the dissociated dislocations in tension and compression induces only an extension of the extrinsic faulted ribbons and concluded that twinning may occur by the propagation of extrinsic stacking faults. Furthermore the energy required for the nucleation of a single twin is minimum when the twin nucleus is composed only of pile-up extrinsic faults [3].

The aim of this paper is to confirm this assumption. Single crystals of a low stacking fault ($\gamma = 10$ mJ/m^2) Cu-13.7 atomic% Al have been studied in compression along the ⟨111⟩ direction. Contrary to previous observations, twinning occurs and starts in this crystal just after the critical shear stress. The low value of γ induces widely dissociated dislocations, so that each partial can propagate individually and independently of the other. The compression stress induced on the partial dislocations extends the extrinsic faulted ribbons and reduces the intrinsic ones, so that extended extrinsic faults are available to form twins at the beginning of the strain [4].

It is not possible to determine by transmission electron microscopy the nature of the constitutive fault of a single twin. However, a strongly different step structure composed of narrow bands of inclined planes is created at the surface, depending on the nature of these stacking faults. The atomic-scale resolution offered by scanning probe microscopy [5–7] allows the analysis of this fine slip line structure and thus to differentiate between the two possible twin mechanisms in this material.

2 Experimental procedure

Compression samples of CuAl single crystal were prepared by cutting and mechanical polishing, and subsequently immersed in a chemical solution to clean the surface. The sample dimensions are nominally $2.5 \times 2.5 \times 5$ mm^3 with a compression axis lying along the [111] direction and a $(11\overline{2})$ observation surface plane. The primary slip system in FCC materials is the $\{111\}\langle 110\rangle$ with a Burgers vector of $a/2\langle 110\rangle$. Step formation is expected therefore to lie along the [312], [132] and [110] directions at $\pm$ 22.2° and 90° respectively from the compression axis (Fig. 1).

The samples were deformed at a rate of approximately 1.6×10^{-5} s^{-1} (Fig. 2) in an apparatus described elsewhere [8,9] and which consists of a micro-compression machine interfaced with an atomic force microscope. During the experiment, the sample surface is scanned continuously which permits the *in situ* observation of the emergence process of dislocations. This experimental device is

[a] e-mail: coupeau@lmp.univ-poitiers.fr

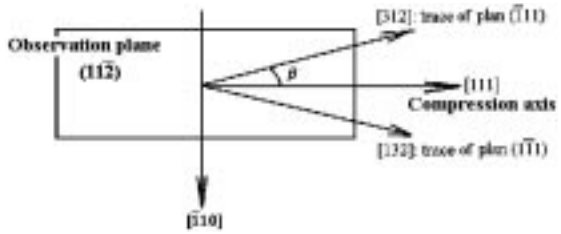

Fig. 1. CuAl specimen configuration.

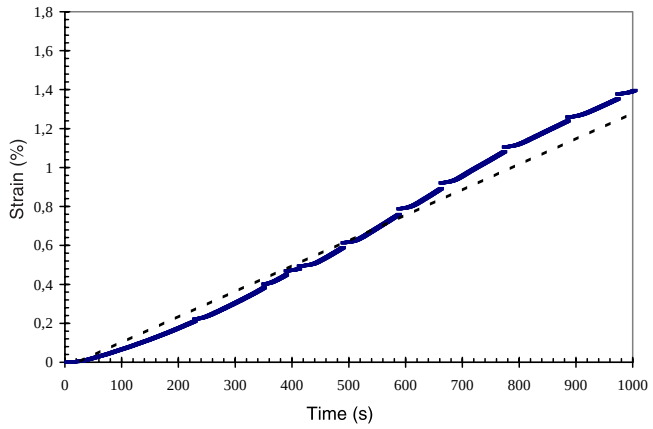

Fig. 2. Deformation rate of the specimen.

particularly suited to the characterization of the surface plastic deformation on a nanometer scale.

Topographical measurements were performed on a commercially available instrument (stand alone atomic force microscopy, *Digital Instruments*) in air at room temperature and pressure. V-shaped cantilevers with a theoretical normal spring constant of 0.1 N/m and sharpened pyramidal silicon nitride tips were used. The images presented were taken from top to bottom along the retrace direction. The compression axis is at about 7° from the horizontal base of each image.

3 Results

The evolution of the sample surface during deformation is seen in Figure 3. The scan size of each image is approximately 16×16 μm^2 (except of image 3b which has been taken at lower size) and the height extension is a few tens of nanometers. Each AFM image is linked to the compression curve, as observed in Figure 4. The critical shear stress is around 30 MPa and the irregularities observed on the curve is accounted for by both the slight drift of the piezo-actuators and the sample stress relaxation, after each stop of the apparatus. The arrows provide the basis for the comparison of the images and the strain values are indicated below. The initial state is shown in Figure 3a; the surface is obviously not perfectly flat with a roughness R_q of 15.1 nm, almost certainly due to preferential chemical etching. Nevertheless, the emergence of the first few dislocations is clearly distinguishable with the appearance of slip lines at 29.5° from the horizontal line, which corresponds to the [132] direction. Only one slip system seems to be activated as often observed.

Several materials, such as LiF or MC2 superalloy phase γ have been studied previously, in which plastic deformation occurs by perfect dislocation propagation [10]. In this case, surface plastic deformation is characterized by a gradual appearance of slip lines. Contrary to these observations, a whole band structure composed of several slip lines seen in Figure 3b suddenly appears characterizing the twin mechanism. Then the increase of stress induces a step by step widening of the twinned *micro-band* (Figs. 3c–3e). In the following, we call twin *micro-band*, a cluster of surface steps resulting from the twin mechanisms; several *individual* twins are thus clustered to form a twin *micro-band*, as seen in the topographical image presented in Figure 5. A limited slip line lying along the [312] direction is also observed in this image and may be the result of a locking of one part of Shockley dislocations of one individual twin in the bulk crystal. It is worth noting that observations by transmission electron microscopy (Fig. 6) have confirmed the presence of these micro-bands and that twin mechanisms are a main contribution of plasticity in this material [2–4].

Analysis of the slip line structure has been carried out. Figures 7 and 8 show the width and height evolution respectively of the twinned band during deformation. Both curves present horizontal asymptotes involving unambiguously a locking of the twin mechanism at this area for a critical strain value and the displacement of the active plastic zone with the appearance of new structure a few micrometers apart, as seen in Figure 3f (white lines on the upper right corner).

The fine structure of steps and particularly the θ experimental value corresponding to the angle between the twinned and initial surfaces may differentiate between the two possible twin mechanisms in this material. However the residual surface roughness after a classical polishing seems too important to obtain a θ value of high accuracy. The first results show that the experimental θ value, obtained by averaging few consecutive sections perpendicularly to one *individual* twin, ranges from 7 to 20°. An average value θ_a of 12.7° has thus been determined from several *individual* twins.

4 Discussion and conclusions

The theoretical angle θ for extrinsic and intrinsic stacking faults can be derived as follows.

The observed slip lines lie along the [132] direction which corresponds to the $(1\bar{1}1)\langle 110\rangle$ system activation. The Burgers vectors may be dissociated into:

$$DC = D\alpha + \alpha C \qquad \frac{1}{2}[110] = \frac{1}{6}[121] + \frac{1}{6}[21\bar{1}]$$

or

$$DB = D\alpha + \alpha B \qquad \frac{1}{2}[011] = \frac{1}{6}[121] + \frac{1}{6}[\bar{1}12]$$

where $\mathbf{b}^{ex} = \mathbf{D}\alpha$ corresponds to the partial head-dislocation in the case of extrinsic stacking fault, and $\mathbf{b}^{in} = \alpha\mathbf{C}$ (or $\alpha\mathbf{B}$) for the intrinsic case.

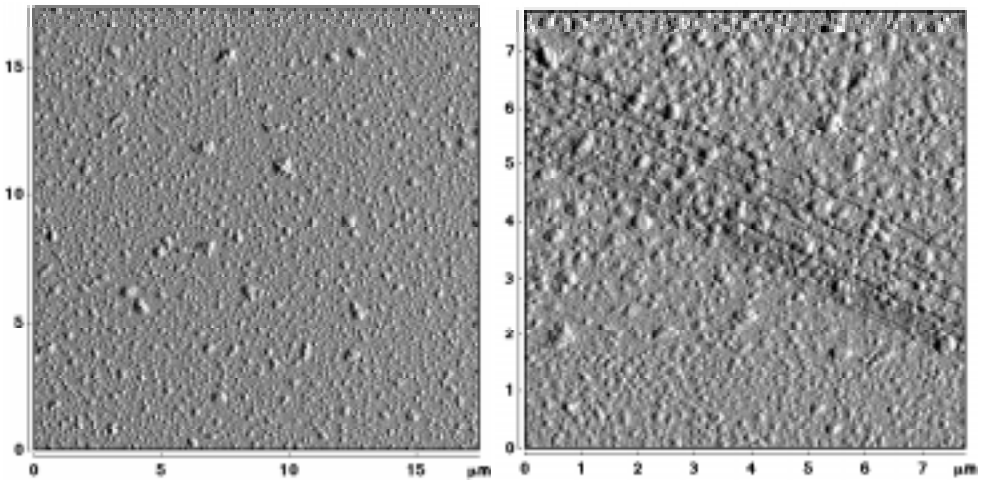

(a) ε=0% (b) ε=0.47%

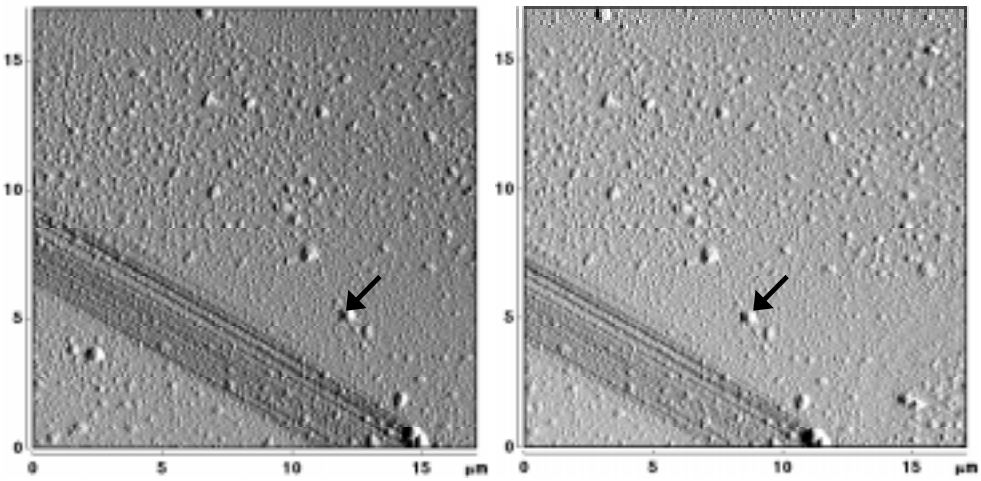

(c) ε=0.79% (d) ε=0.92%

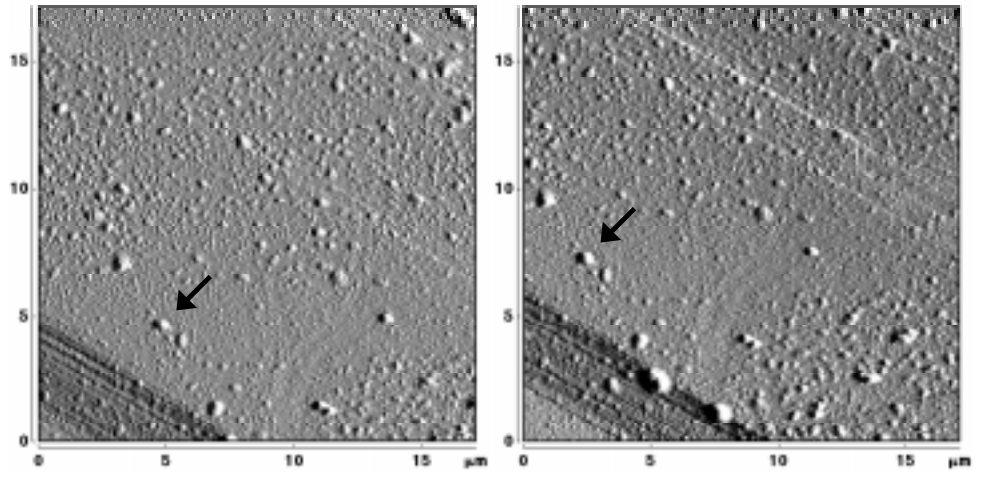

(e) ε=1.10% (f) ε=1.26%

Fig. 3. *In situ* deformed CuAl atomic force micrographs. The AFM images presented here have been taken in error signal mode and the scan size is indicated beside.

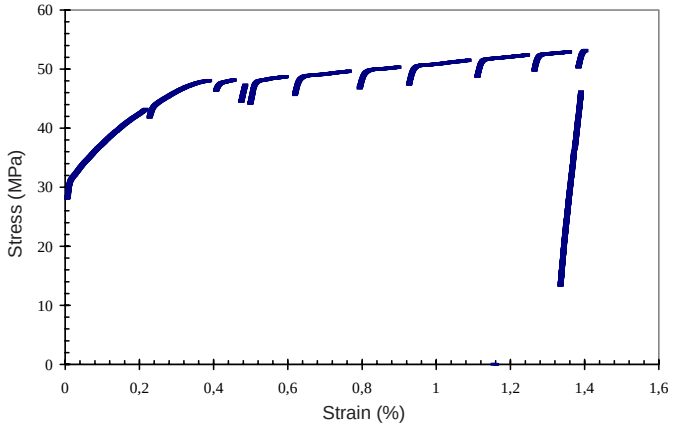

Fig. 4. CuAl stress-strain curve. The discontinuities are explained by both the drift of the piezo-actuator and the sample stress relaxation after each stop of the experimental device.

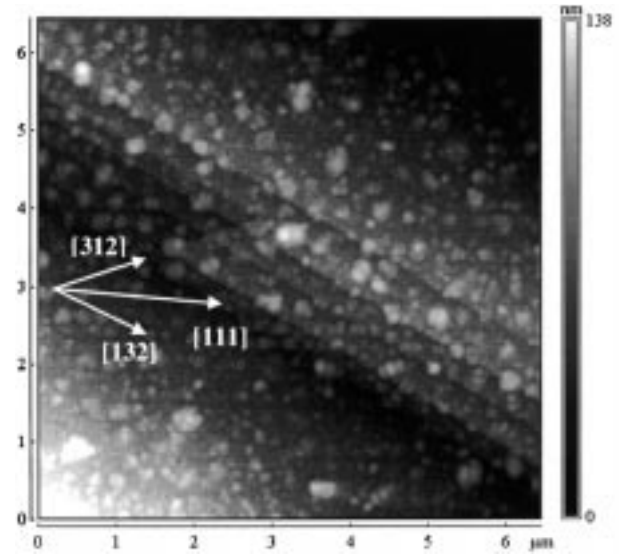

Fig. 5. Twinned band fine structure. The scan size is about 6×6 μm^2 with a height extension of 138 nm.

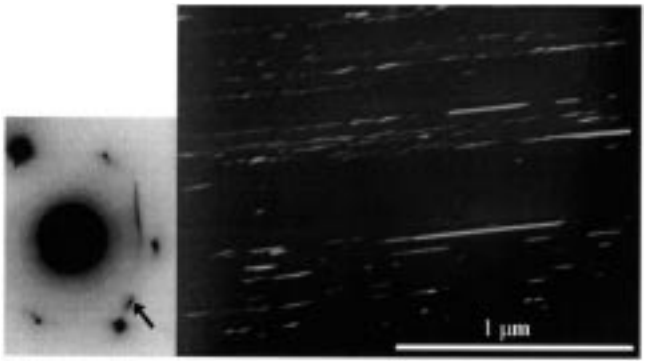

Fig. 6. Bright twins in the bulk CuAl single crystal. The spot (111) used for the TEM micrograph in dark field is indicated by an arrow on the diffraction pattern.

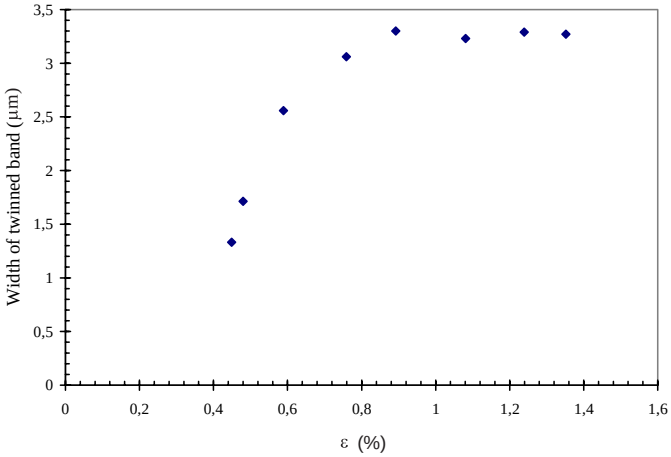

Fig. 7. Twinned micro-band width *vs*. specimen strain.

Projecting Shockley vectors along surface perpendicular $\mathbf{n}_1$, parallel $\mathbf{n}_2$ and perpendicular $\mathbf{n}_3$ slip lines directions leads to:

$$b_1^{\mathrm{ex}} = \mathbf{b}^{\mathrm{ex}} \cdot \mathbf{n}_1 = \frac{1}{6} b_{\mathrm{S}},$$

$$b_1^{\mathrm{in}} = \mathbf{b}^{\mathrm{in}} \cdot \mathbf{n}_1 = \frac{5}{6} b_{\mathrm{S}} \quad \left(\text{or} \;\; b_1^{\mathrm{in}} = \frac{2}{3} b_{\mathrm{S}} \right),$$

$$b_2^{\mathrm{ex}} = \mathbf{b}^{\mathrm{ex}} \cdot \mathbf{n}_2 = \frac{1}{3\sqrt{14}} b_{\mathrm{S}},$$

$$b_2^{\mathrm{in}} = \mathbf{b}^{\mathrm{in}} \cdot \mathbf{n}_2 = \frac{5}{3\sqrt{14}} b_{\mathrm{S}} \quad \left(\text{or} \;\; b_2^{\mathrm{in}} = \frac{4}{3\sqrt{14}} b_{\mathrm{S}} \right),$$

$$b_3^{\mathrm{ex}} = \mathbf{b}^{\mathrm{ex}} \cdot \mathbf{n}_3 = \frac{9}{2\sqrt{21}} b_{\mathrm{S}},$$

$$b_3^{\mathrm{in}} = \mathbf{b}^{\mathrm{in}} \cdot \mathbf{n}_3 = \frac{3}{2\sqrt{21}} b_{\mathrm{S}} \quad \left(\text{or} \;\; b_3^{\mathrm{in}} = \frac{3}{\sqrt{21}} b_{\mathrm{S}} \right),$$

where $\mathbf{n}_1 = (1/\sqrt{6})[11\bar{2}]$, $\mathbf{n}_2 = (1/\sqrt{21})[4\bar{2}1]$, $\mathbf{n}_3 = (1/\sqrt{14})[132]$, $b_S = a/\sqrt{6}$ and a is the lattice parameter.

In the case of extrinsic stacking fault, the twin mechanism involves the propagation of only one partial dislocation along two crystallographic planes (Fig. 9). Hence the θ_{ex} angle is given by the following equations:

$$\tan \theta_{\mathrm{ex}} = \frac{b_1^{\mathrm{ex}}}{2d_{\mathrm{ex}} - b_2^{\mathrm{ex}}},$$

$$d_{\mathrm{ex}} = \frac{\sqrt{2}}{\sin \varphi_{\mathrm{ex}}} b_{\mathrm{S}},$$

$$\tan \varphi_{\mathrm{ex}} = \frac{b_1^{\mathrm{ex}}}{b_2^{\mathrm{ex}}} \cdot$$

One obtains $\theta_{\mathrm{ex}} = 3.06°$

Twin mechanism may also be accounted for by the propagation of only one Shockley dislocation along each

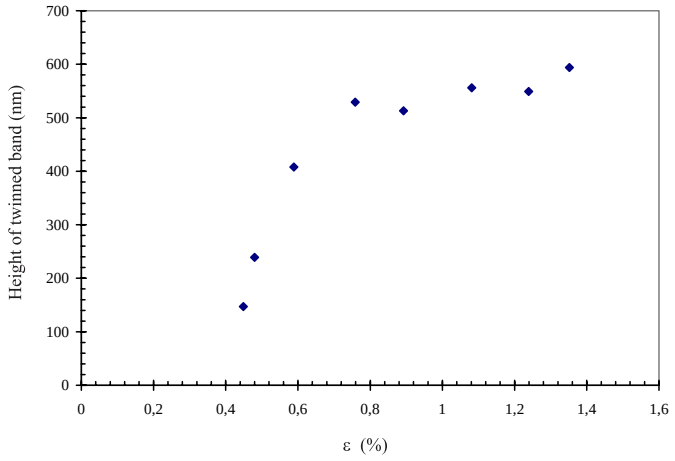

Fig. 8. Twinned micro-band height *vs*. specimen strain.

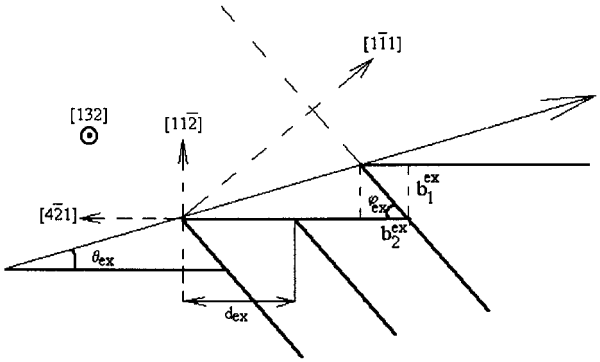

Fig. 9. Extrinsic stacking fault twin mechanism (not drawn at the right scale).

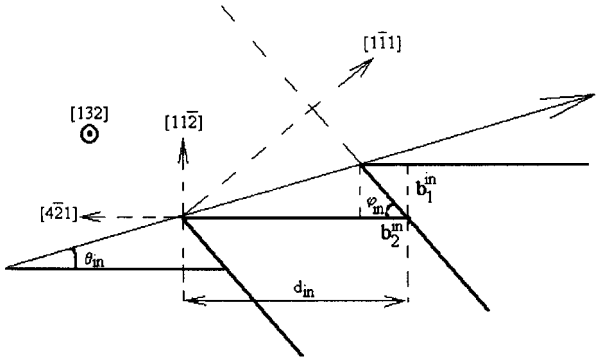

Fig. 10. Intrinsic stacking fault twin mechanism (not drawn at the right scale).

crystallographic plane creating an intrinsic stalking fault (Fig. 10). $\theta_{\rm in}$ is defined as follows:

$$\tan\theta_{\rm in} = \frac{b_1^{\rm in}}{d_{\rm in} - b_2^{\rm in}},$$
$$d_{\rm in} = \frac{\sqrt{2}}{\sin\varphi_{\rm in}} b_{\rm S},$$
$$\tan\varphi_{\rm in} = \frac{b_1^{\rm in}}{b_2^{\rm in}}\,.$$

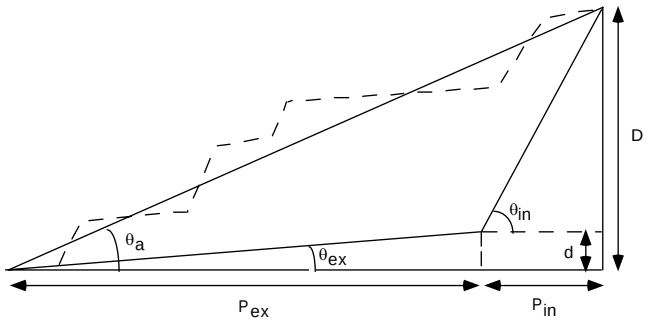

Fig. 11. Schematic representation of the respective contributions $P_{\rm in}$ and $P_{\rm ex}$ of each mechanism in twinning.

This leads to $\theta_{\rm in} = 35.8°$ (or 31.9°) depending on the Burgers vector.

In the present study, the crystallographic orientations of the applied stress and the observation face are such that the angles between the inclined faces of the twinned bands and the initial surface plane have very different theoretical values, depending on the nature of the stacking fault, intrinsic (in) or extrinsic (ex). It should be noted that the same angular range is found for the two cases of intrinsic stacking fault, compared to the case of extrinsic for which this parameter is considerably lower.

From the previous results, the following conclusions can be emphasized: the extrinsic mechanism alone is not possible, because θ would be about 3° or smaller. It is here worth noting that the resolution of the images used for the analysis, that is the distance between two experimental points, is around 10 nm. As the thickness of the studied twins is around the same order of magnitude than those observed by transmission electron microscopy [11], the possibility of unresolved fine structure composed of *nanotwins* separated by undeformed regions has to be rejected. It is thus concluded that *individual* twins are not also created by the intrinsic mechanism alone; both extrinsic and intrinsic stacking faults have to be taken into account. The respective contributions $P_{\rm ex}$ and $P_{\rm in}$ of each mechanism (ex or in) occurring during twinning can be deduced from the average $\theta_{\rm a}$ value obtained on one *individual* twin, as shown in Figure 11. One therefore obtains:

$$P_{\rm in} = \frac{\tan\theta_{\rm a} - \tan\theta_{\rm ex}}{\tan\theta_{\rm in} - \tan\theta_{\rm ex}},$$
$$P_{\rm ex} = 1 - P_{\rm in}.$$

A $\theta_{\rm in} = 33.8°$ (average of the two possible intrinsic mechanism) is used for the calculation which leads to $P_{\rm in}$ =25.8% and $P_{\rm ex}$ =74.2%. These first results show that about 75% of the twinning occurs *via* extrinsic mechanism.

Improvement of both the resolution the images and the initial surface features by high vacuum AFM investigations, to provide a more accurate θ measurement, should confirm the possibility of twin mechanisms in CuAl (13.7%) alloy by the propagation of Shockley dislocations creating extrinsic stacking faults in the bulk crystal.

This work was partially supported by the DRET agency and the Région Poitou-Charentes. The authors would like to thank L. Cartz for fruitful discussions and useful suggestions.

References

1. F. Tranchant, J. Vergnol, J. Grilhé, Script. Met. Mat. **17**, 175 (1983).
2. F. Tranchant, Ph.D. thesis, University of Poitiers, France, 1987.
3. J. Vergnol, J. Grilhé, J. Phys. France **45**, 1479 (1984).
4. F. Tranchant, J. Vergnol, M.F. Denanot, J. Grilhé, Script. Met. **21**, 269 (1987).
5. G. Binnig, H. Rohrer, C. Gerber, E. Weibel, Phys. Rev. Lett. **50**, 120 (1983).
6. G. Binnig, C.F. Quate, C. Gerber, Phys. Rev. Lett. **56**, 9 (1986).
7. F.J. Giessibl, G. Binnig, Ultramicroscopy **42-44**, 7 (1992).
8. M.K. Small, C. Coupeau, J. Grilhé, Script. Met. Mat. **32**, 1573 (1995).
9. C. Coupeau, J.C. Girard, J. Grilhé, J. Vacuum Sci. Tech. (in press, 1999).
10. C. Coupeau, J.C. Girard, J. Grilhé, Probe Microscopy (in press, 1999).
11. J. Vergnol, Ph.D. thesis, University of Poitiers, France, 1980.